A 0–55-GHz Coplanar Waveguide to Coplanar Strip Transition

Dimitrios E. Anagnostou, *Member, IEEE*, Matt Morton, *Student Member, IEEE*, John Papapolymerou, *Senior Member, IEEE*, and Christos G. Christodoulou, *Fellow, IEEE*

***Abstract*—A broadband coplanar waveguide (CPW) to coplanar strip (CPS) transmission line transition directly integrated with an RF microelectromechanical systems reconfigurable multiband antenna is presented in this paper. This transition design exhibits very good performance up to 55 GHz, and uses a minimum number of dissimilar transmission line sections and wire bonds, achieving a low-loss and low-cost balancing solution to feed planar antenna designs. The transition design methodology that was followed is described and measurement results are presented.**

***Index Terms*—Antenna feed, coplanar strip (CPS), coplanar stripline, coplanar waveguide (CPW), transition.**

I. Introduction

ADVANCES IN reconfigurable antenna technology and RF microelectromechanical systems (RF-MEMS) switches have recently established new frontiers in antenna design. In [1], Anagnostou *et al.* developed a multiband reconfigurable self-similar antenna, demonstrating the performance enhancement that can be achieved with the use of self-similar (or pre-fractal) antenna designs. A significant issue in the applicability and research of such conformal dipole antennas is their feeding method. Any balanced antenna can be fed using a balanced transmission line. The currents flowing on this line are equal and out-of-phase from the generator to the antenna's feed point. If the line is unbalanced, reflections at the antenna's terminals cause unequal currents to flow on the transmission line (usually on the outer conductor of the coaxial cable), which radiate in an unpredictable manner, resulting in distorted asymmetrical patterns and erroneous voltage standing-wave ratio (VSWR) measurement.

To balance a transmission line, a *balun*, a device that allows only the *differential* mode of the currents to pass through, must be placed between the feeding cable and the antenna's terminals. Baluns are often narrowband, and thus can feed planar narrowband dipoles. However, to feed wideband or multiband antennas, a transition (balun) capable of balancing the transmission line in a much broader range of frequencies is needed. Such baluns work by tapering the coaxial ground slowly into a single-tip conductor, forming a two-wire transmission line at its termination [2].

For our application though, the reconfigurable antenna (shown in [1, Fig. 13]), which covers various frequencies from 8 to 25 GHz, is fabricated on a quarter of a silicon wafer with feed dimensions 300 × 360 μm. Any intervention or via on the dielectric layers at such small scales would affect the antenna performance by a large degree. As a result, the transition needs to be both wideband and planar in order to feed the antenna from the same plane. All the above led to the development of the coplanar waveguide (CPW) to coplanar strip (CPS) transmission line transition described below.

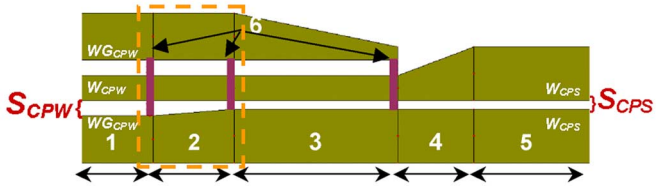

1) S-CPW: Symmetric coplanar waveguide,
2) T-CPW: Tapered (asymmetric) coplanar waveguide, tapered linearly in the lower slot to match the CPS slot for Z_0=50Ω. This section will be eliminated.
3) A-CPW: Asymmetric coplanar waveguide tapered linearly in the upper strip to match the upper width of the symmetric CPS at the next step's end.
4a) U-SLO (top) Unterminated slotline open. Capacitive effect between this and the upper conductor of the strip line in the next step should be minimal.
4b) T-CPS (bottom) Tapered (asymmetric) coplanar strip transmission line tapered linearly in the upper strip until it becomes symmetric.
5) S-CPS Symmetric coplanar strip transmission line, used to feed the antenna.
6) Wire-bonds connecting the ground at each discontinuity to suppress the non-CPW modes and balance the transmission line.

Fig. 1. Layout of a typical CPW to CPS transition with three air-bridges or wire bonds from [3].

II. Design Concepts

First, a 20-GHz CPW–CPS transition similar to the one in [3] was designed as shown in Fig. 1. The transition is comprised from a series of symmetric and asymmetric transmission line sections. An "air-bridge" or wire bond is needed before each asymmetric section discontinuity to suppress any non-CPW mode and retain the balance on the transmission line. The slot of the CPS (S_{CPS}) needs to be tapered to match the width of the one of the two slots of the symmetric CPW (S_{CPW}), as illustrated in section 2 of Fig. 1.

Manuscript received January 19, 2006; revised June 10, 2007. This work was supported in part by the Georgia Electronic Design Center, by the National Science Foundation under Grant ECS 0218732 and Grant EPSCoR 0554609, and by the Mission Research Corporation under Contract SC-0244-0008, UNM-1.

D. E. Anagnostou is with the Electrical Engineering Department, South Dakota School of Mines and Technology, Rapid City, SD 57701 USA (e-mail: danagn@ieee.org).

M. Morton and J. Papapolymerou are with the School of Electrical and Computer Engineering, Georgia Institute of Technology, Atlanta, GA 30308 USA (e-mail: head23@gmail.com; papapol@ece.gatech.edu).

C. G. Christodoulou is with the Electrical and Computer Engineering Department, University of New Mexico, Albuquerque, NM 87106 USA (e-mail: christos@ece.unm.edu).

Color versions of one or more of the figures in this paper are available online at http://ieeexplore.ieee.org.

Digital Object Identifier 10.1109/TMTT.2007.911909

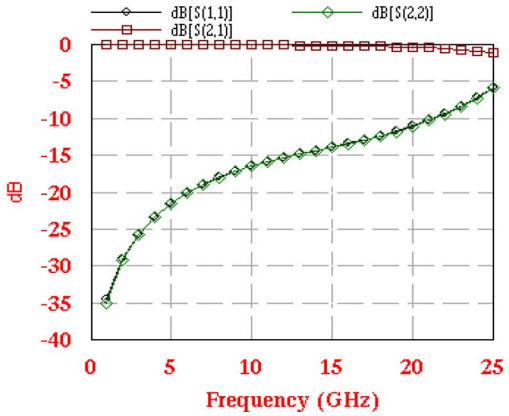

Fig. 2. Simulated S-parameters of the back-to-back initial transition with 600-μm-long lines showed very good response up to 20 GHz. A gradual performance decline at higher frequencies can be noticed.

The simulated frequency response is shown in Fig. 2, where a gradual performance decline at higher frequencies can be noticed as the return loss becomes smaller than 10 dB. To satisfy the design goals and increase the transition bandwidth, several alterations were made.

A reduction in the number of discontinuities can lead to a reduction in the number of wire bonds. This reduction can be achieved by careful consideration of the characteristics of the beginning and ending slots (CPS transmission line slot S_{CPS} and CPW slot S_{CPW}, respectively), as shown in Fig. 1. For this purpose, we need to place a restriction in the design that for all CPW and the CPS sections, all slots should be of equal width. By applying this restriction, the slot of section 1 (S_{CPW}) can be designed to be equal to S_{CPS} in sections 3–5. One discontinuity of the transmission line and one wire bond (section 2) are then redundant and eliminated. Sections 1 and 2 are unified and the air-bridges of sections 2 and 3 are the only ones needed.

This imposes the design of CPW and CPS transmission line sections with the exact same slot width (and equal to S_{CPS}), while maintaining the same characteristic impedance throughout the transition to minimize reflections, which can be challenging.

It is possible to adjust the CPW line by varying the widths of its signal conductor (W_{CPW}) and of its slot (S_{CPW}) such that its characteristic impedance remains relatively constant and equal to that of the CPS transmission line in order to eliminate the need for taper. When the CPW slot width (S_{CPW}) is increased, the line's characteristic impedance (Z_{0_CPW}) increases as well. On the other hand, increasing the signal conductor's width (W_{CPW}) causes Z_{0_CPW} to decrease. It is a straightforward conclusion to presume that several combinations of slot and signal conductor widths can lead to a CPW with a specific value of characteristic impedance. This value is equal to the CPS's characteristic impedance, and depends upon the application's design specifications, probe pitch, and fabrication equipment's tolerance and capabilities. Here, a 150-μm-pitch CPW line was used to match with the dimensions from other parts of the system and the RF probes.

This methodology was also used to match and balance the reconfigurable antenna of [1] to $Z_{\mathrm{in}} = 50\ \Omega$, maintaining a

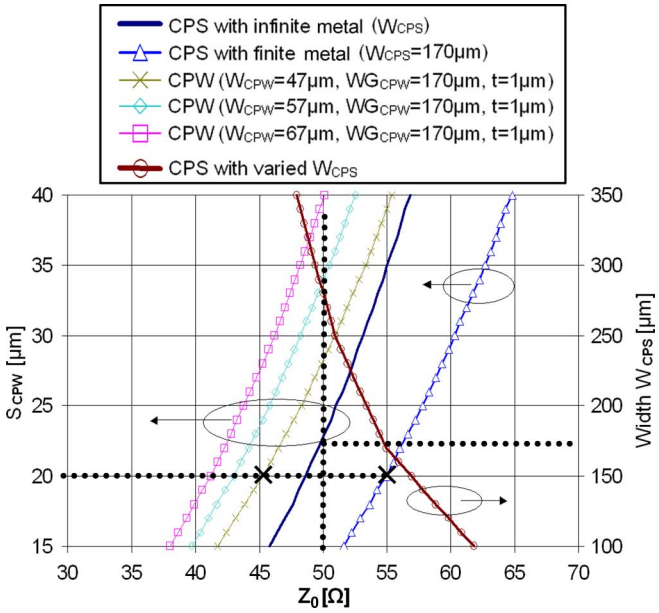

Fig. 3. CPS and CPW line characteristic impedance as it varies with the slot width (S_{CPW} or S_{CPS}) and the width of the metal conductor (W_{CPS} for the CPS line). A 20-μm slot was used in the CPS line plot.

VSWR $\leq$ 1.25 throughout the transition. It can also be extended to other impedance values due to the fact that the CPS line's characteristic impedance (Z_{0_CPS}) is strongly dependent upon its slot's width (S_{CPS}), while the CPW's characteristic impedance (Z_{0_CPW}) depends both on the CPW slot's width (S_{CPW}) and the width of its signal conductor (W_{CPW}), adding one degree of freedom to the design. Some relations between the characteristic impedance (Z_0) of the different lines used here versus the width of their slot (S_{CPW}, assuming $S_{\mathrm{CPS}} = S_{\mathrm{CPW}}$) are shown in Fig. 3 (left y-axis).

1) Increasing the width of the CPW slot (S_{CPW}), increases the characteristic impedance of the CPW line, as illustrated for three different CPW lines with $W_{\mathrm{CPW1}} = 47\ \mu$m, $W_{\mathrm{CPW2}} = 57\ \mu$m, and $W_{\mathrm{CPW3}} = 67\ \mu$m, with $WG = 171\ \mu$m.
2) Increasing the width of the center conductor of the CPW lines (W_{CPW}) decreases their characteristic impedance.
3) Increasing the width of the CPS slot (S_{CPS}) increases the CPS transmission line's characteristic impedance.
4) At the same time, a finite-metal CPS transmission line has higher Z_0 than the (theoretically) infinite-metal CPS transmission line with the same slot width (S_{CPS}).

By varying the width of the metal part of the CPS line (W_{CPS}) while maintaining the width of its slot (S_{CPS}) constant and equal to that of the CPW line (i.e., $S_{\mathrm{CPS}} = S_{\mathrm{CPW}}$), one can alter the CPS transmission line's characteristic impedance to match that of the CPW line with the same slot width (S_{CPW}). Thus, the lines dimensions can be adjusted for uniform characteristic impedance throughout the transition.

Fig. 3 shows the variety of CPW choices one can use in a transition for a specific CPS line slot width ($S_{\mathrm{CPS}} = S_{\mathrm{CPW}}$), which cannot be significantly varied. For example, this is achieved by drawing a vertical line from $Z_0 = 50\ \Omega$ and noting all CPW and CPS lines that are crossed, as long as these lines in the graph have been extracted for the same slot width $S_{\mathrm{CPS}} = S_{\mathrm{CPW}} =$

TABLE I
SUBSTRATE CROSS SECTION

Position	Layer Type	Thickness	Material
1 (Top)	Air	-	-
2	Metal 1	2 μm	Gold
3	Dielectric 3	0.3 μm	Silicon Nitride
4	Dielectric 2	1 μm	Silicon Dioxide
5	Dielectric 1	400 μm	Silicon
6 (Bottom)	Air	-	-

20 μm). In Fig. 3, all three shown CPW transmission lines can have $Z_{0\_\mathrm{CPW}} = 50\ \Omega$, and any of the three shown signal conductor widths (W_{CPW}) can be used with their appropriate slot widths given by the left y-axis. The CPS line curves are also drawn for various slot dimensions (S_{CPS}) and an approximate match can be extracted in a visual manner.

In particular, for the design described in this study, not all lines intersected at the same points and, thus, a perfect match was not achieved. We have used a $Z_{0\_\mathrm{CPW}} = 45\ \Omega$ CPW line characteristic impedance with $S_{\mathrm{CPW}} = 20\ \mu$m slot width, which also defined the slot width of the CPS transmission line (S_{CPS}). A CPS transmission line with this slot width and finite metal width of $W_{\mathrm{CPS}} = 171\ \mu$m has characteristic impedance $Z_{0\_\mathrm{CPS}} = 55\ \Omega$, marked with "×" at (55 Ω, 20 μm) on Fig. 3.

The quality of matching for different dimensions and impedances can be "visually" extracted from the distance of the curves (S_{CPW} versus Z_0), between two different transmission line curves. The closer the curves are, the better the match. For specific impedance and slot width values, this is equivalent to how close the two "×" marks are in Fig. 3.

To improve matching, the CPS transmission line could be designed with a lower $Z_{0\_\mathrm{CPS}} = 50\ \Omega$ if wider metal ($W_{\mathrm{CPS}} = 270\ \mu$m) was used, as indicated from the right y-axis of Fig. 3, where the plotted curve is for the CPS transmission line used here with $S_{\mathrm{CPS}} = 20\ \mu$m. For different S_{CPS} widths, different curves can be plotted to enable designs with other characteristic impedances. The CPW line could also achieve a $Z_{0\_\mathrm{CPW}} = 50\ \Omega$ with a gap of 28 μm, but this would result in larger CPS transmission line characteristic impedance (Z_{0_CPS}). Analytical equations as functions of elliptic integrals [6] were used to obtain starting points for the CPS and CPW transmission lines. The lines were then simulated with a method of moments electromagnetic simulator.[1] Fig. 3 can always be used as a starting point, as it gives dimensions and values for the transition sections, neglecting any mutual coupling with other system components. The final dimensions are described in Section III and were chosen as a compromise between the desired impedance matching, a good overall system performance, while taking into account the limits of the fabrication equipment.

To minimize fabrication complexity and maximize co-process compatibility with the integration of the RF-MEMS, the transition is fabricated on a high-resistive Si wafer, and made with the same metallization and patterning steps as the antenna. Underneath the metal (Au) layer, there are thin layers of SiO_2 and Si_3N_4, as imposed by the design of the switches. The sequence of dielectric and metallization layers is shown in Table I.

[1]IE3D is a registered trademark of the Zeland Corporation, Fremont, CA.

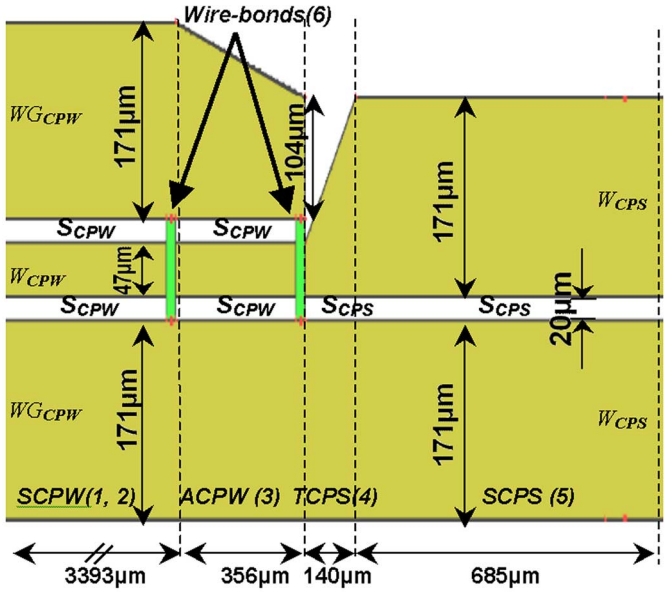

Fig. 4. Final CPW–CPS transition with dimensions and names of the different transmission line sections as defined in Fig. 1. The total length of the back-to-back configuration was $2 \cdot 4300 = 8600\ \mu$m.

This transition design is improved when compared to existing ones [3]–[5] in the sense that it uses a reduced number of discontinuities (and, thus, wire bonds), leading to better RF performance with wider bandwidth, faster fabrication time, lower loss, and lower cost.

III. BACK-TO-BACK TRANSITION DESIGN AND SIMULATIONS

Using the methodology described in Section II, the broadband transition was designed and its structure is shown in Fig. 4. The design procedure begins at section 5 (CPS), going towards section 1 (CPW). A slot of $S_{\mathrm{CPS}} = 20\ \mu$m in section 5 is used and maintained constant. Additionally, the dimensions of the bottom strip are also kept constant during the entire transition. In section 4, the upper strip of the CPS transmission line is linearly narrowed to the center strip of the CPW line, and a tapered CPW ground is added next beginning from the width of the top CPS strip until the CPW line becomes symmetric. Both CPW slots are maintained constant at $S_{\mathrm{CPW}} = 20\ \mu$m and the transition ends in a symmetric CPW design.

The CPS line slot (S_{CPS}) and its conductors' width (W_{CPS}) were calculated first and a width $W_{\mathrm{CPS}} = 171\ \mu$m was used to bring Z_{0_CPS} close to 50 Ω. The guide wavelength was found to be $\lambda_g = 15.3$ mm at 7.75 GHz, $\lambda_g = 8$ mm at 15 GHz, and $\lambda_g = 4.81$ mm at 24.75 GHz. The calculated effective dielectric constant was $\varepsilon_{r\_\mathrm{eff}} = 6.35$. The final design layout is shown in Fig. 4, and detailed in Table II, along with the transition of Fig. 1.

The keen reader may notice some differences between the theoretical "optimum" values that can be extracted from Fig. 3 and the values used here. These can be attributed to the use of the method of moments software for the fine tuning of the transition integrated with the antenna in order to achieve not only wide bandwidth, but also a good system performance. Also, the method of moments software, while it takes into account any discontinuity effects that analytical equations might disregard, it neglected the finiteness of the dielectric substrates, extending

TABLE II
DIMENSIONS OF THE CPW–CPS TRANSITIONS (IN MICROMETERS)

T. L. Type	Length L (1-5)		Strip Width W_{CPW}, W_{CPS}		Slot Width S_{CPW}, S_{CPS}		Ground Plane Width WG_{CPW}	
	Init.*	Final	Init.*	Final	Init.*	Final	Init.*	Final
SCPW	203	3393	80	47	49.00	20	150	171
TCPW	203	---	80	---	Top: 49 Bot.:49 - 28	---	Top: 150 Bot.:150 - 171	---
ACPW	406	356	80	47	Top: 49 Bot.:49 - 28	20	Top: 150 Bot.:150 - 171	Top: 171 - 104 Bottom: 171
TCPS	190	140	Top: 80 -171 Bottom: 171	Top:47 -171 Bottom:171	28	20	---	---
SCPS	314	685	171	171	28	20	---	---
Wire bonds	16	25	Left:178 Right:156	87	---	---	---	---

*"Init." is the 0–20-GHz transition, as illustrated in Fig. 1, modified for silicon substrate.

them to infinity. This resulted in significant (but not detrimental) differences between simulation and measurements, at such dimension (micrometer) scales.

The transition as integrated with the antenna was attached to a 3400-μm-long CPW transmission line section to connect to the RF probes. This way, the RF probe head was kept far from the antenna and its effect in the radiation pattern was minimal.

The simulated frequency response of the transition in a back-to-back configuration is shown in Fig. 5. The performance is very good from dc up to 40 GHz, covering the desired antenna resonant frequencies, and exhibiting very low insertion loss. In the back-to-back configuration, return loss is greater than 12 dB, while insertion loss is less than 2.8 dB (value at 23 GHz), which implies that some minimal radiation takes place, as the overall length gets electrically larger. Additionally, the back-to-back transmission coefficient's insertion phase is almost linear, resulting in minimal distortion of the RF signal from the input until the antenna terminals. Finally, simulations showed that expected values for the integrated (single) transition return loss and insertion loss were 15 and 1.3 dB, respectively. The measured results are discussed in Section IV.

IV. BACK-TO-BACK TRANSITION MEASUREMENTS

The transition's performance can be partially evaluated by the measured results of the reconfigurable antenna system that it was integrated with, as shown in [1, Figs. 13–15]. A magnified photograph of the integrated transition (Fig. 6) shows a slightly misplaced (right) manual wire bond. The S_{11} measurement in [1, Fig. 13] showing some fluctuations emphasize the effort presented here and justify the need to reduce the number of wire bonds on transition designs. In a mass-production application, the more accurate MEMS air-bridges can substitute wire bonds with better performance.

In order to obtain a complete characterization, the transition was also fabricated in a separate silicon wafer in a back-to-back configuration, at the cleanroom facilities of the Georgia Institute of Technology, Atlanta, using standard photolithography techniques and equipment.

The transition is directly connected to different transmission line sections (CPW and CPS), which may add ohmic and substrate losses in the circuit. As any measurement will incorporate these losses, a correct evaluation of the transition's performance can be made by subtracting them from the measured S_{21}. To do so, transitions with different CPW and CPS transmission line lengths were fabricated and measured. Losses induced by or related to the thin metal layer of Au, surface roughness, and dielectric that were related to these transmission line sections were calculated.

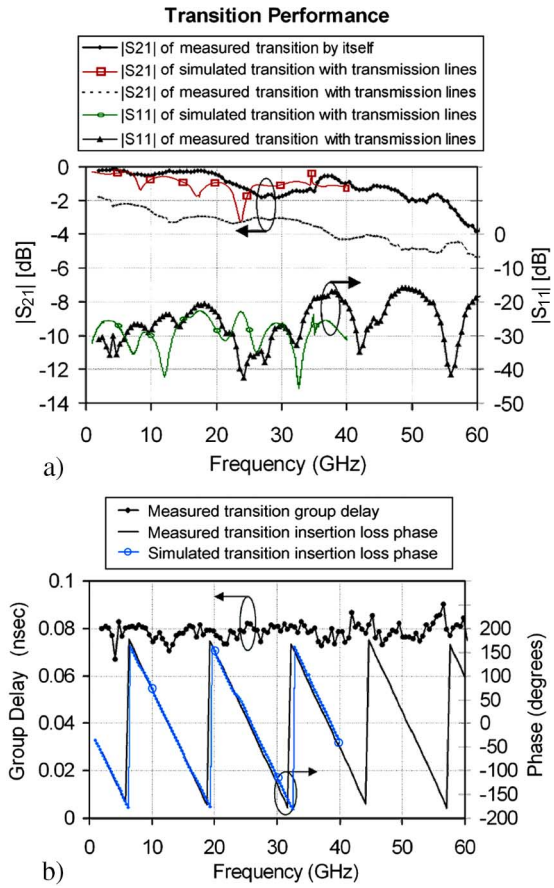

Fig. 5. Measured and simulated back-to-back transition performance. (a) Magnitude of insertion loss and reflection coefficient. (b) Group delay and insertion phase of S_{21} for the transition with all transmission lines attached.

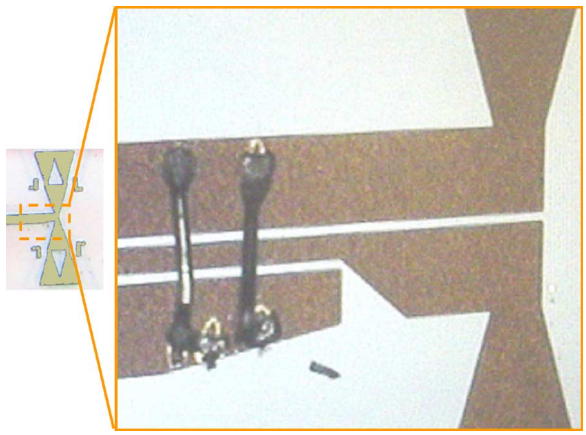

Fig. 6. Fabricated transition integrated with the antenna.

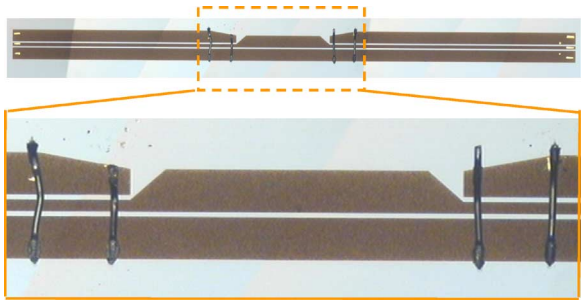

Fig. 7. Photograph and magnification of the fabricated CPW–CPS transition with the transmission line sections attached.

The CPW line loss per unit length was calculated from a CPW line used in the calibration. The loss, in decibels/micrometer, for every frequency was found, and from that, the loss of the entire CPW line section was derived and subtracted from the overall transition's performance. Next, the loss of the CPS line section was found in a similar way.

The calculated transition losses are also shown in Fig. 5(a) within the measured range from 0 to 60 GHz. With the back-to-back configuration, a low-loss performance was obtained from 2 GHz up to 55 GHz since the insertion loss is less than 1.9 dB. The bandwidth exceeded the expected simulated frequency range. Additionally, the insertion phase and group delay of the propagated signal were measured and calculated, respectively. Both are plotted in Fig. 5(b). The insertion phase varies in a linear way with frequency, as expected, while the group delay is fairly constant with values between 0.067–0.090 ns, an average value $m = 0.078$ ns, and small variance $\sigma^2 = 0.12 \cdot 10^{-3}$ ns^2. A photograph of the back-to-back fabricated transition is shown in Fig. 7, where the transition itself is shown magnified to better illustrate the structure's details.

A comparison between simulated and measured results shows relatively good agreement in $|S_{11}|$. The largest deviation was found at 24 and 37 GHz with $\pm 7\ \Omega$, which is a small variation when considering the complexity of the structure, the different layers, and the modeling of the wire bonds. The insertion phase was linear and very similar both in the simulation and measurement. Some variation in $|S_{21}|$ can be noticed. The electromagnetic fields are mostly concentrated in the space between the metallic conductors so an edge meshing was used. Results in this case are sensitive to the edge mesh's size and density, as well as the wire bonds and the conducting properties of the sputtered Au. All conductors were simulated as perfect, which is also another reason for the observed difference. These differences though were expected and proved to be noncritical for the successful outcome of this study.

The major advantage of this design when compared to previous ones is its broader bandwidth, which is obtained using a reduced number of wire bonds. The design approach presented may also be used for transmission lines with different values of characteristic impedance. The one presented here exhibits very good performance up to 55 GHz with a reduced number of transmission line discontinuities achieving a low-loss and low-cost method to feed planar antenna designs fabricated on rigid substrates. The transition was directly integrated with an RF-MEMS reconfigurable multiband antenna and exhibited very good results as well. Finally, by replacing the wire bonds with accurately placed and less lossy MEMS air-bridges, and by minimizing the lengths of the CPW and CPS line sections, transition designs with larger bandwidth and very low loss can be developed.

REFERENCES

[1] D. E. Anagnostou, G. Zheng, M. Chryssomallis, J. Papapolymerou, C. G. Christodoulou, J. Lyke, and G. Ponchak, "Design, fabrication and measurements of a self-similar re-configurable antenna with RF-MEMS switches," *IEEE Trans. Antennas Propag. (Special Issue)*, vol. 54, no. 2, pt. 1, pp. 422–432, Feb. 2006.

[2] J. W. Duncan and V. P. Minerva, "100 : 1 bandwidth balun transformer," *Proc. IRE*, vol. 48, no. 2, pp. 156–164, Feb. 1960.

[3] S. G. Mao, C. T. Hwang, R. B. Wu, and C. H. Chen, "Analysis of coplanar waveguide-to-coplanar stripline transitions," *IEEE Trans. Microw. Theory Tech.*, vol. 48, no. 1, pp. 23–29, Jan. 2000.

[4] T. Chiu, "A building-block design scheme for planar transmission-line transitions," *Proc. Inst. Elect. Eng.—Microw., Antennas, Propag.*, vol. 150, pt. 6, pp. 405–410, 2003.

[5] A. T. Kolsrud, M.-Y. Li, and K. Chang, "Dual-frequency electronically tunable CPW-fed CPS dipole antenna," *Electron. Lett.*, vol. 34, no. 7, pp. 609–611, Apr. 1998.

[6] B. C. Wadell, *Transmission-Line Design Handbook*. Norwood, MA: Artech House, 1991, pp. 83–84.

Dimitrios E. Anagnostou (S'98–M'05) was born in Athens, Greece, in November 1975. He received the Diploma degree in electrical and computer engineering, from the Democritus University of Thrace, Thrace, Greece, in 2000, and the M.Sc. and Ph.D. degrees in electrical engineering from the University of New Mexico, Albuquerque, in 2002 and 2005, respectively.

From 2005 to 2006, he was a Post-Doctoral Fellow with the School of Electrical and Computer Engineering, Georgia Institute of Technology, Atlanta. In 2007, he joined the faculty of the Electrical Engineering Department, South Dakota School of Mines and Technology, Rapid City, as an Assistant Professor. He has authored or coauthored over 30 peer-reviewed international journal and conference publications. He has filed two invention disclosures on reconfigurable and ultra-wideband (UWB) antennas. His current research involves direct-write printing for the development and integration of RF circuits on flexible substrates (liquid crystal polymer (LCP), Kapton), reconfigurable and low-cost flexible antennas and RF front-ends, novel antenna designs, microwave packaging, RF-MEMS, neural networks, and image processing.

Dr. Anagnostou is a member of Eta Kappa Nu and the Technical Chamber of Greece. He was the recipient of three research and travel grants from 2003 to 2005. He served as a session chair at the IEEE Antennas and Propagation Society (IEEE AP-S) 2006 and 2007 International Symposia. He serves as a reviewer for the IEEE TRANSACTIONS ON ANTENNAS AND PROPAGATION and the IEEE TRANSACTIONS ON MICROWAVE THEORY AND TECHNIQUES.

Matt Morton (S'02) received the B.S. degree in electrical and computer engineering from the University of Kansas, Lawrence, in 2002, and the M.S. and Ph.D. degrees in electrical engineering from the Georgia Institute of Technology, Atlanta, in 2003 and 2007, respectively.

His research interests include SiGe X-band phase shifters for monolithic radar transmit/receive (T/R) modules, low-cost RF CMOS receiver design, RF-MEMS phase shifters, broadband RF-MEMS switch packaging, low-temperature RF-MEMS packaging techniques on organic liquid crystal polymer (LCP), metamaterial crosstalk isolators, and nanoparticle magnetic thin films.

John Papapolymerou (S'90–M'99–SM'04) received the B.S.E.E. degree from the National Technical University of Athens, Athens, Greece, in 1993, and the M.S.E.E. and Ph.D. degrees from The University of Michigan at Ann Arbor, in 1994 and 1999, respectively.

From 1999 to 2001, he was an Assistant Professor with the Department of Electrical and Computer Engineering, University of Arizona, Tucson. During the summers of 2000 and 2003, he was a Visiting Professor with the University of Limoges, Limoges, France. From 2001 to 2005, he was an Assistant Professor with the School of Electrical and Computer Engineering, Georgia Institute of Technology, Atlanta, where he is currently an Associate Professor. He has authored or coauthored over 140 publications in peer-reviewed journals and conferences. His research interests include the implementation of micromachining techniques and MEMS devices in microwave, millimeter-wave and terahertz circuits and the development of both passive and active planar circuits on semiconductor (Si/SiGe, GaAs) and organic substrates [liquid-crystal polymer (LCP), low-temperature co-fired ceramic (LTCC)] for system-on-a-chip (SOC)/system-on-package (SOP) RF front ends.

Dr. Papapolymerou is the vice-chair for Commission D of the U.S. National Committee of URSI. He is an associate editor for IEEE MICROWAVE AND WIRELESS COMPONENT LETTERS and the IEEE TRANSACTIONS ON ANTENNAS AND PROPAGATION. During 2004, he was the chair of the IEEE Microwave Theory and Techniques (MTT)/Antennas and Propagation (AP) Atlanta Chapter. He was the recipient of the 2004 Army Research Office (ARO) Young Investigator Award, the 2002 National Science Foundation (NSF) CAREER Award, the Best Paper Award presented at the 3rd IEEE International Conference on Microwave and Millimeter-Wave Technology (ICMMT2002), Beijing, China, and the 1997 Outstanding Graduate Student Instructional Assistant Award presented by the American Society for Engineering Education (ASEE), The University of Michigan at Ann Arbor Chapter. His student was also the recipient of the Best Student Paper Award presented at the 2004 IEEE Topical Meeting on Silicon Monolithic Integrated Circuits in RF Systems, Atlanta, GA.

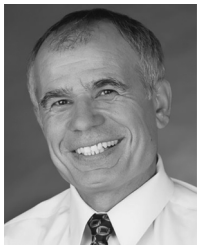

Christos G. Christodoulou (S'80–M'81–SM'90–F'02) received the B.Sc. degree in physics and math from the American University of Cairo, Cairo, Egypt, in 1979, and the M.S. and Ph.D. degrees in electrical engineering from North Carolina State University, Raleigh, in 1981 and 1985, respectively.

From 1985 to 1998, he was a faculty member with the University of Central Florida, Orlando. In 1999, he joined the Electrical and Computer Engineering Department, University of New Mexico, Albuquerque, where he was Chair of this department from 1999 to 2005. He is an Associate Editor of the *International Journal of RF and Microwave Computer-Aided Engineering*. He was a Guest Editor for the Special Issue on "Applications of Neural Networks in Electromagnetics" of the Applied Computational Electromagnetics Society's *ACES Journal*. He has authored or coauthored over 250 papers in journals and conferences. He has authored or coauthored 12 book chapters and coauthored four books. His research interests are modeling of electromagnetic systems, reconfigurable systems, machine learning applications in electromagnetics, and smart antennas.

Dr. Christodoulou is a member of Eta Kappa Nu, The Electromagnetics Academy (TEA), and Commission B of the United States National Committee of the International Union of Radio Science (USNC/URSI). He served as the general chair of the IEEE Antennas and Propagation Society (AP-S)/URSI 1999 Symposium, Orlando, FL, as the co-chair of the IEEE 2000 Symposium on Antennas and Propagation for Wireless Communications, Waltham, MA, and the co-technical chair for the IEEE AP-S/URSI 2006 Symposium, Albuquerque, NM. He is currently an associate editor for the IEEE TRANSACTIONS ON ANTENNAS AND PROPAGATION and the *IEEE Antennas and Propagation Magazine*. He was appointed an IEEE AP-S Distinguished Lecturer for 2007 to 2009 and was elected vice-chair for the Albuquerque IEEE Antennas and Propagation (AP)/Microwave Theory and Techniques (MTT) Chapter.